J. Chem. Lett. 7 (2026) 290-312

Research Article

Journal of Chemistry Letters
journal homepage: www.jchemlett.com
ISSN (online) 2717-1892 (print) 2821-0123

Integrated molecular docking and ADMET-based computational investigation of potent phytochemicals from multiple medicinal plants as CYP2E1 inhibitors

Mamidi Srinivas[1], Madda Jyothi[2], K. Ramesh[3,*], Sabeena Hussain Syed[4], Nithin Kumar Pallepati[5], J. Priyanga[6], Ashutosh Pathak[7], E. Joel Mart[6]

[1]*Department of Chemistry, Government Polytechnic, P. O. Box: 508202, Nagarjunasagar, Telangana, India.*
[2]*Department of Chemistry, Government Polytechnic, P. O. Box: 509216, Shadnagar, Telangana, India.*
[3]*Department of Chemistry, Government Degree College, P. O. Box: 502313, Narsapur, Medak, Telangana, India.*
[4]*School of Pharmacy, Vishwakarma University, Betal Nagar, Kondhwa, P. O. Box: 411048, Pune, Maharashtra, India.*
[5]*Amneal Pharmaceuticals, 50 Horseblock Road, P. O. Box: 11719, Brookhaven, New York, United States.*
[6]*Department of Pharmacology, School of Pharmaceutical Sciences, Vels Institute of Science, Technology and Advanced Studies (VISTAS), Pallavaram, P. O. Box: 600117, Chennai, Tamil Nadu, India.*
[7]*Department of Pharmacy Practice, Teerthanker Mahaveer College of Pharmacy, Teerthanker Mahaveer University, P. O. Box: 244001, Moradabad, Uttar Pradesh, India.*

ARTICLE INFO

Article history:
Received 30 April 2026
Received in revised form 04 June 2026
Accepted 11 June 2026

Keywords:
CYP2E1 inhibition
Molecular docking
ADMET analysis
Phytochemicals
In-silico drug discovery

ABSTRACT

Cytochrome P450 2E1 (CYP2E1) is a heme-containing monooxygenase involved in xenobiotic metabolism and oxidative stress generation, making it a significant therapeutic target. The present study aimed to identify potent natural inhibitors of CYP2E1 through an integrated molecular docking and ADMET-based computational approach. Twenty structurally diverse phytochemicals were selected from medicinal plants based on reported pharmacological relevance. Molecular docking was performed to evaluate binding affinity and interaction stability within the CYP2E1 active site. Docking results demonstrated that several compounds effectively occupied the catalytic pocket and interacted with key residues such as CYS437, ILE115, LEU368, ALA299, VAL364, and PHE430. Shatavarin IV exhibited the highest binding affinity (–12.9 kcal/mol), surpassing the native ligand (–12 kcal/mol), followed by Amygdalin (–10.2 kcal/mol). Withaferin A, Curcumin, Galangin, Aloe-emodin, and Ferulic acid also exhibited favorable hydrogen-bonding and hydrophobic interaction profiles within the active site, suggesting potential CYP2E1 inhibitory activity based on computational predictions. Comprehensive ADMET analysis revealed important pharmacokinetic differences among the candidates. Although Shatavarin IV displayed superior docking performance, its high molecular weight and polarity suggested limited oral absorption. In contrast, Ferulic acid, Curcumin, Aloe-emodin, and Withaferin A demonstrated balanced physicochemical properties, improved intestinal absorption, acceptable metabolic profiles, and comparatively lower toxicity risks. Overall, Ferulic acid emerged as the most promising candidate when both binding efficiency and pharmacokinetic suitability were considered, warranting further experimental validation. Future studies should focus on molecular dynamics simulations and in vitro/in vivo validation to confirm stability, efficacy, and safety profiles.

1. Introduction

Cytochrome P450 2E1 (CYP2E1) is a key member of the cytochrome P450 superfamily, a group of heme-containing monooxygenases responsible for the metabolism of endogenous substrates and xenobiotics [1–3]. CYP2E1 plays a particularly important role in the oxidation of low-molecular-weight compounds, including ethanol, anesthetics, and environmental toxins. A distinguishing feature of this enzyme is its high

* Corresponding author E-mail: ramesh.chemou@gmail.com
https://doi.org/10.22034/jchemlett.2026.580491.1401

capacity to generate reactive oxygen species (ROS) during the catalytic turnover. Excessive ROS production contributes to oxidative stress, lipid peroxidation, inflammation, and cellular injury, which are closely associated with liver diseases, metabolic disorders, neurodegenerative conditions, and carcinogenesis [4,5]. Consequently, the selective inhibition of CYP2E1 has gained increasing attention as a therapeutic strategy to reduce oxidative damage and toxin-mediated tissue injury.

Natural products derived from medicinal plants have long been considered valuable sources of therapeutic agents [6]. Flavonoids such as quercetin represent an important class of phytochemicals with diverse biological activities and well-characterized structural, physicochemical, and redox properties [7]. Phytochemicals, such as flavonoids, phenolic acids, terpenoids, alkaloids, saponins, and quinones, possess diverse biological activities, including antioxidant, anti-inflammatory, hepatoprotective, and enzyme-modulating effects. Medicinal plants are particularly rich sources of phytochemicals with antioxidant properties, supporting their continued evaluation as sources of pharmacologically relevant bioactive compounds [8]. Their structural diversity and functional group variability provide significant potential for interactions with enzyme active sites [9]. Many plant-derived compounds have been shown to modulate cytochrome P450 enzymes, suggesting that they may serve as safer and more effective alternatives or adjuncts to synthetic inhibitors. However, despite the growing interest in natural CYP modulators, comprehensive comparative investigations of structurally diverse phytochemicals on CYP2E1 remain limited. Most available studies focus on individual compounds, specific plant extracts, or a single phytochemical class, providing only a restricted understanding of their relative inhibitory potential and drug-like characteristics.

Despite their therapeutic promise, systematic evaluation of numerous phytochemicals using conventional experimental approaches is time-consuming and resource-intensive. Advances in computational drug discovery have enabled the efficient virtual screening of large compound libraries, allowing the rapid identification of promising candidates prior to experimental validation. Computational investigations can provide valuable molecular-level insights into the structural, electronic, physicochemical, and interaction characteristics of biologically relevant molecules and drug-related systems [10]. In particular, structure-based computational strategies facilitate the prediction of molecular interactions between ligands and target proteins, providing insights into binding affinity, stability, and potential inhibitory mechanisms [11, 12]. Furthermore, early prediction of pharmacokinetic and toxicity properties is essential to minimize late-stage drug development failure [10]. Integrating molecular interaction analysis with pharmacokinetic evaluation provides a rational framework for prioritizing compounds with strong target affinity and favorable drug-like characteristics [13]. This approach is particularly valuable in natural product research, where structural complexity and variability may influence absorption, metabolism, and safety profiles [10].

Although molecular docking and ADMET prediction have been widely employed in natural product research, studies integrating a broad spectrum of phytochemicals from multiple medicinal plants for comparative CYP2E1 inhibitor screening are scarce. A systematic evaluation of compounds belonging to different chemical classes can provide valuable insights into common binding patterns, key interacting residues, and the relationship between binding affinity and pharmacokinetic suitability. Such comparative analyses are important for identifying candidates with effective target engagement and favorable drug development potential.

Therefore, the present study aimed to perform an integrated computational investigation of 20 structurally diverse bioactive phytochemicals selected from multiple medicinal plants to explore their potential as CYP2E1 inhibitors. By combining molecular docking with comprehensive ADMET profiling, this study aimed to identify potent CYP2E1-binding phytochemicals and prioritize candidates based on their pharmacokinetic and safety characteristics. This integrated multi-plant screening approach provides a broader comparative assessment than conventional single-compound or single-plant investigations and may facilitate the identification of promising natural compounds for the development of effective CYP2E1-modulating therapeutic agents. The selected medicinal plants and their representative phytochemicals are shown in Figure 1.

2. Materials and Methods

2.1. Selection of phytochemical compounds

The phytochemical compounds selected for the present computational investigation were based on documented pharmacological relevance, reported bioactivity, and the availability of well-characterized chemical constituents from medicinally important plants (Table 1). Each plant species was screened through a literature analysis to identify its major bioactive compounds with potential therapeutic significance. The final selection focused on one potent representative phytoconstituent from each plant to ensure diversity in terms of chemical structure and biological activity.

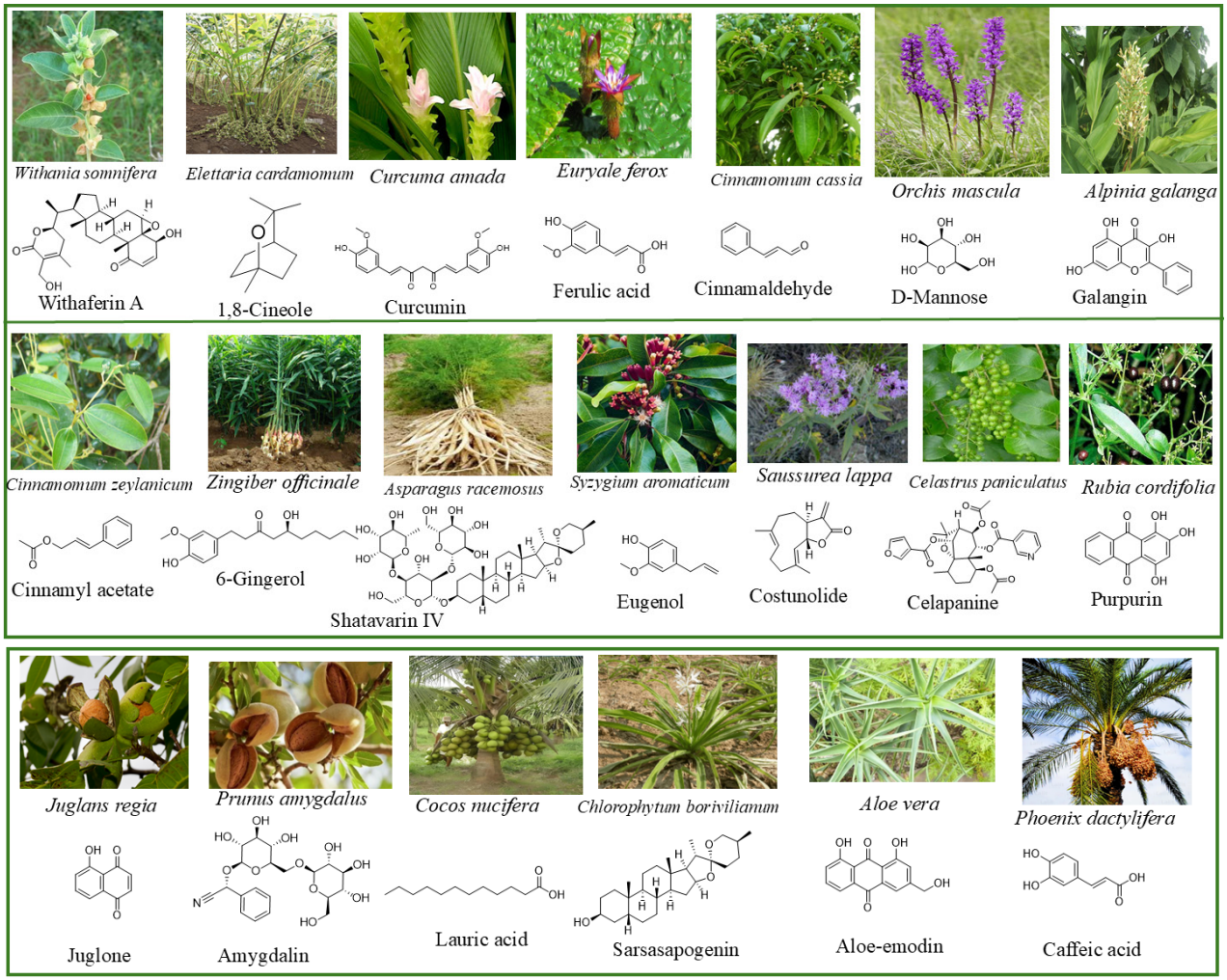

Fig. 1. Comprehensive representation of selected medicinal plants and their corresponding bioactive phytochemicals employed in the study, highlighting the structural diversity of compounds screened for CYP2E1 inhibitory potential.

Withaferin A was selected from Withania somnifera because of its well-established anti-inflammatory and antioxidant properties [14]. Elettaria cardamomum contributes 1,8-Cineole (Eucalyptol), a major volatile compound known for its pharmacological activity [15]. Curcumin was selected as the principal bioactive compound from Curcuma amada because of its strong antioxidant and enzyme-modulating potential [16]. Ferulic acid was selected from Euryale ferox [17], and cinnamaldehyde was identified as the key compound from Cinnamomum cassia [18].

D-Mannose was selected from Orchis mascula based on its biochemical importance [19,20]. Galangin, a flavonoid with known biological activity, was selected from Alpinia galanga [21]. Cinnamyl acetate was identified as the representative compound from Cinnamomum zeylanicum [22], whereas 6-Gingerol was selected from Zingiber officinale because of its prominent therapeutic properties [23].

Shatavarin IV, a steroidal saponin, was selected from Asparagus racemosus for its reported bioactivity [24]. Eugenol, the principal phenolic compound, was selected from the Syzygium aromaticum [25]. Costunolide was identified from Saussurea lappa, and celapanine was selected from Celastrus paniculatus based on its pharmacological significance [26,27]. Purpurin was isolated from Rubia cordifolia, and juglone was identified from Juglans regia [28,29]. Amygdalin was selected from Prunus amygdalus because of its known biological relevance [30]. Lauric acid was included as the key fatty acid from Cocos nucifera, whereas sarsasapogenin was chosen from Chlorophytum borivilianum [31,32]. Aloe-emodin was selected from Aloe vera, and caffeic acid was identified as a major phenolic constituent of Phoenix dactylifera [33,34]. Thus, a structurally diverse panel of 20 phytochemicals representing different chemical classes, such as alkaloids, flavonoids, phenolics, terpenoids, fatty acids, saponins, and quinones, was selected for further molecular docking and computational evaluation. This systematic selection ensured a comprehensive screening of bioactive natural compounds with potential inhibitory activity.

Table 1. Plants and their most potent compounds with their chemical structures

Plant	Final Identified Potent Compound	Chemical Structures
Withania somnifera	Withaferin A	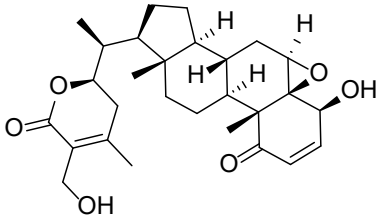
Elettaria cardamomum	1,8-Cineole (Eucalyptol)	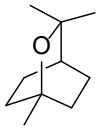
Curcuma amada	Curcumin	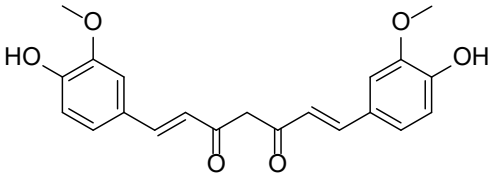
Euryale ferox	Ferulic acid	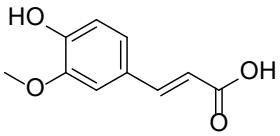
Cinnamomum cassia	Cinnamaldehyde	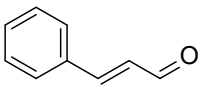
Orchis mascula	D-Mannose	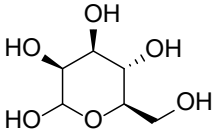
Alpinia galanga	Galangin	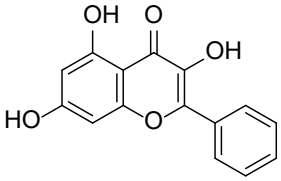
Cinnamomum zeylanicum	Cinnamyl acetate	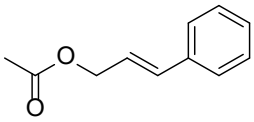
Zingiber officinale	6-Gingerol	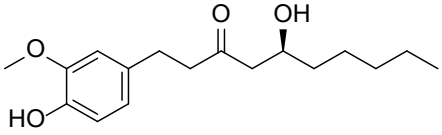
Asparagus racemosus	Shatavarin IV	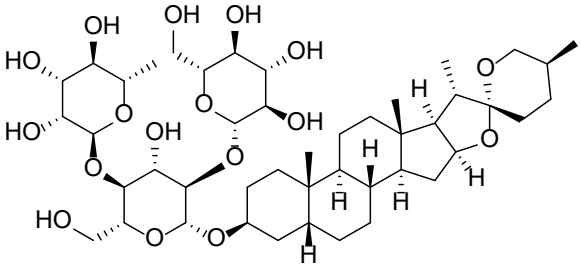

Plant	Final Identified Potent Compound	Chemical Structures
Syzygium aromaticum	Eugenol	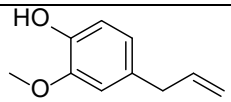
Saussurea lappa	Costunolide	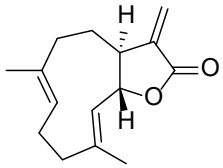
Celastrus paniculatus	Celapanine	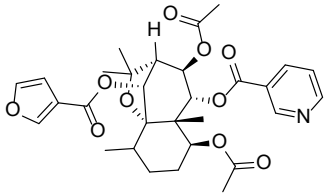
Rubia cordifolia	Purpurin	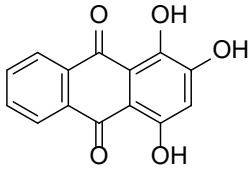
Juglans regia	Juglone	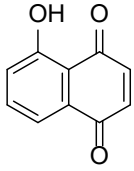
Prunus amygdalus	Amygdalin	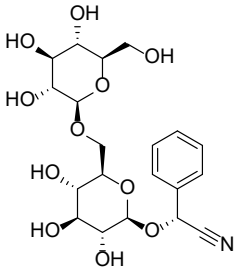
Cocos nucifera	Lauric acid	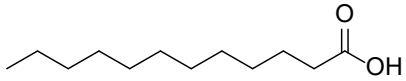
Chlorophytum borivilianum	Sarsasapogenin	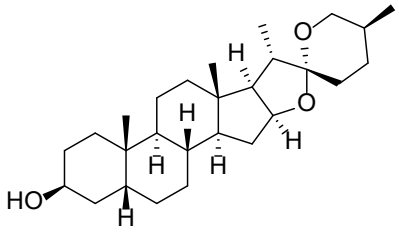
Aloe vera	Aloe-emodin	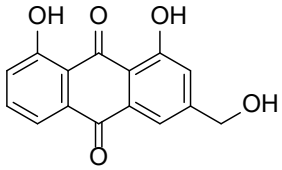
Phoenix dactylifera	Caffeic acid	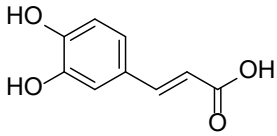

2.2. Molecular docking

Molecular docking was performed using the X-ray crystal structure of Human Cytochrome P450 2E1 (CYP2E1) obtained from the RCSB Protein Data Bank (PDB ID: 3T3Z) (Figure 2). CYP2E1 is a phase I xenobiotic-metabolizing enzyme involved in the oxidative metabolism of ethanol, drugs, and procarcinogens and is associated with oxidative stress and hepatotoxicity. The protein structure was prepared by removing co-crystallized ligands, water molecules, and heteroatoms, followed by the addition of polar hydrogens and appropriate charge assignments. Gasteiger charges were assigned, and nonpolar hydrogens were merged using AutoDock Tools prior to conversion. The prepared structure was converted to the PDBQT format. Ligand structures were drawn using ChemDraw, and their three-dimensional conformations were retrieved from PubChem in SDF format. All ligands were geometry-optimized and energy-minimized prior to docking and converted into PDBQT format using the MMFF94 force field with energy minimization until the convergence criteria were achieved [35–39].

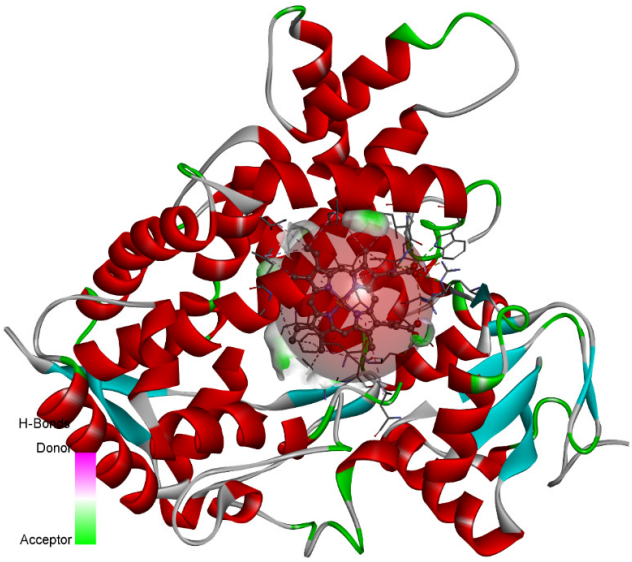

Fig. 2. 3D ribbon representation of CYP2E1 enzyme with native ligand

Docking simulations were performed using PyRx 0.8, incorporating the AutoDock Vina 1.1.2 algorithm. A grid box was defined around the active site based on the co-crystallized ligand position, with center coordinates set at X = 26.242093, Y = 24.632163, and Z = 8.001372, with grid box dimensions of 25 × 25 × 25 Å to adequately cover the catalytic-binding pocket. Docking was performed using an exhaustiveness value of 8, with a maximum of 9 binding poses generated per ligand, and multiple poses were generated. The best binding conformation was selected based on the lowest binding energy and a favorable orientation within the catalytic pocket. Although RMSD-based re-docking validation was not performed, the docking protocol was standardized by maintaining consistent grid parameters, scoring functions, and ligand preparation procedures for all compounds, and the results were comparatively interpreted relative to the native ligand to ensure internal consistency and reliability. Protein–ligand interactions were analyzed using BIOVIA Discovery Studio Visualizer to identify hydrogen bonds, hydrophobic interactions, π-interactions, and other non-covalent forces stabilizing the complexes with uniform visualization and interaction criteria applied across all docked complexes [40–43].

2.3. ADMET Analysis

The ADMET properties of the selected phytochemicals were evaluated using an in silico approach. The chemical structures were drawn and verified using ChemDraw, and structural data, including canonical SMILES, were obtained from PubChem. The drug-likeness and physicochemical parameters, such as molecular weight, logP, TPSA, hydrogen bond donors and acceptors, rotatable bonds, and solubility, were predicted using SwissADME, applying Lipinski's Rule of Five and Veber's criteria. Comprehensive pharmacokinetic and toxicity predictions were performed using ADMETlab 3.0, including gastrointestinal absorption, BBB permeability, P-glycoprotein interaction, CYP450 metabolism, clearance, hepatotoxicity, Ames mutagenicity, and carcinogenicity [44–47]. The predicted parameters were comparatively analyzed to identify compounds with favorable pharmacokinetic behaviors and acceptable safety profiles for further studies.

3. Results and Discussion

3.1. Molecular docking

Molecular docking analysis was performed to evaluate the binding affinity and interaction patterns of the selected phytochemicals against Cytochrome P450 2E1 (CYP2E1) and to compare their inhibitory potential with that of the native ligand. CYP2E1 is a heme-containing monooxygenase enzyme involved in xenobiotic metabolism and oxidative stress generation, and its inhibition is considered therapeutically significant. Docking scores, intermolecular interactions, and ligand energies were analyzed to determine the binding stability and interaction strength within the active site. The binding interactions and docking scores are shown in Table 2. The 2D and 3D interactions are listed in Table 3. All interaction analyses were performed using a consistent docking protocol and uniform visualization criteria to ensure the comparability of all ligands.

The native ligand exhibited a strong docking score of –12 kcal/mol with a ligand energy of 987.76 kcal/mol,

indicating stable binding within the CYP2E1 active pocket. It formed multiple conventional hydrogen bonds, predominantly with CYS437 (bond distances ranging from 2.45 to 2.80 Å), along with additional interactions with LEU368, ILE115, TRP122, and ARG126. Hydrophobic stabilization was extensive, including Pi-sigma interactions with PHE430, Alkyl interactions with LEU296 and VAL364, and Pi-Alkyl interactions with ALA299 and ALA443. A notable π-sulfur interaction with CYS437 further strengthened the complex. The residues CYS437, ILE115, LEU368, ALA299, VAL364, and PHE430 were identified as key interacting residues because they were consistently observed across multiple ligand–protein complexes (Table 2).

Among the tested phytochemicals, Shatavarin IV demonstrated the highest docking score of –12.9 kcal/mol, surpassing the native ligand and indicating a superior binding affinity. It formed multiple strong hydrogen bonds with GLY300 (1.90 Å), THR304 (1.70 Å), GLY439, and ILE180, suggesting tight anchoring to the active site. In addition, extensive hydrophobic interactions with CYS437, ALA299, LEU368, and PHE207 contributed to the stability of the complex. The presence of multiple hydrogen bonds and hydrophobic contacts suggests favorable binding to the CYP2E1 active site.

Amygdalin also exhibited a strong docking score of –10.2 kcal/mol, forming several conventional hydrogen bonds with PRO429, ASN367, ARG435, and ARG126. Hydrophobic interactions with LEU368 and CYS437, along with a pi-sulfur interaction, further stabilized the complex. Although its binding affinity was slightly lower than that of the native ligand, the diversity and number of hydrogen bonds suggest a strong interaction potential. Withaferin A showed a docking score of –8.7 kcal/mol and formed a conventional hydrogen bond with GLN358, along with hydrophobic interactions involving LEU368, VAL364, CYS437, and PHE430 residues. Similarly, Curcumin (–8.6 kcal/mol) exhibited predominantly hydrophobic π-alkyl interactions with LEU363, VAL364, LEU368, and ALA443, indicating that hydrophobic forces played a major role in its binding stability rather than hydrogen bonding. These interaction trends are consistent with the binding patterns summarized in Table 2 and should be interpreted comparatively with respect to the native ligand. Galangin (–8.5 kcal/mol) and purpurin (–8.0 kcal/mol) demonstrated balanced interaction profiles involving both hydrogen bonding and hydrophobic contacts. Galangin formed a strong hydrogen bond with GLN358 (2.26 Å) and hydrophobic interactions with LEU363 and CYS437, whereas purpurin interacted through hydrogen bonding with ASN367 and Pi interactions with ALA438 and LEU368. Aloe-emodin (–8.3 kcal/mol) and ferulic acid (–8.1 kcal/mol) also showed stable binding patterns, forming hydrogen bonds with residues such as ILE115, CYS437, ARG435, and TRP122, which are similarly involved in native ligand stabilization, indicating overlapping binding regions. These overlapping interaction profiles suggest that these compounds occupy a similar binding region within the catalytic pocket.

Moderate binding affinities were observed for compounds such as costunolide (–8.0 kcal/mol) and juglone (–7.2 kcal/mol), which primarily engaged in hydrophobic and π–π interactions with aromatic residues such as PHE430 and LEU363. In contrast, weaker binding scores were recorded for 1,8-Cineole (–6.0 kcal/mol), cinnamaldehyde (–6.0 kcal/mol), cinnamyl acetate (–6.5 kcal/mol), eugenol (–6.6 kcal/mol), D-mannose (–5.8 kcal/mol), lauric acid (–5.8 kcal/mol), and sarsasapogenin (–4.2 kcal/mol). These compounds exhibited limited hydrogen bonding and primarily relied on hydrophobic interactions, which may explain their comparatively lower binding affinities. The reduced interaction diversity observed for these compounds correlates with their comparatively lower docking scores, as presented in Table 2. The selected phytochemicals exhibited considerable variation in molecular size, polarity, flexibility, and overall physicochemical properties, which may have influenced the docking outcomes and predicted binding energies. Compounds such as Shatavarin IV and Amygdalin possess substantially higher molecular weights and greater hydrogen-bonding capacities than smaller molecules such as ferulic acid, Curcumin, and Aloe-emodin. Consequently, the higher docking scores observed for larger compounds may partly reflect their increased ability to establish multiple interactions within the binding pocket, rather than necessarily indicating greater biological potency. Therefore, docking scores should be interpreted as comparative indicators of binding potential and interaction patterns, rather than as definitive measures of inhibitory activity. To address this limitation, ADMET analysis was employed to provide a more comprehensive assessment of both the binding affinity and drug-likeness characteristics. Overall, several phytochemicals were predicted to occupy the catalytic pocket of CYP2E1 and interact with key residues, including CYS437, ILE115, LEU368, ALA299, VAL364, and PHE430. Among the screened compounds, Shatavarin IV and Amygdalin exhibited the most favorable docking scores, whereas Withaferin A, Curcumin, Galangin, Aloe-emodin, and Ferulic acid demonstrated notable interaction profiles within the active site. These findings suggest the potential CYP2E1 inhibitory activity of the selected phytochemicals based on computational predictions. However, the results should be considered preliminary and require further validation through molecular dynamics simulations, in vitro enzymatic inhibition assays, and other experimental studies to confirm the binding stability and biological efficacy.

Table 2. Binding interactions of all selected compounds with CYP2E1 enzyme

Amino Acid	Bond Length	Bond Type	Bond Category	Ligand Energy (Kcal/mol)	Docking Score
Native Ligand					
CYS437	2.52991	Hydrogen Bond	Conventional Hydrogen Bond	987.76	-12
CYS437	2.80844				
CYS437	2.53106				
LEU368	2.86759				
ILE115	3.0965				
TRP122	2.41122				
ARG126	2.32465				
LEU368	2.65272				
ILE115	3.38852		Carbon Hydrogen Bond		
ALA438	2.60899		Pi-Donor Hydrogen Bond		
PHE430	3.68839	Hydrophobic	Pi-Sigma		
CYS437	2.45621	Other	Pi-Sulfur		
LEU296	4.82462	Hydrophobic	Alkyl		
ALA299	4.47225				
ALA443	3.51158				
VAL364	3.50681				
LEU393	5.39361				
ILE114	4.01061				
ILE115	4.694				
LEU296	5.23981				
ALA438	3.4255				
PRO429	4.64197				
LEU442	3.94024				
ALA443	3.52345				
ALA299	4.74038		Pi-Alkyl		
ALA299	4.04044				
CYS437	4.62595				
CYS437	4.22904				
ALA443	4.94955				
VAL364	5.24833				
LEU368	5.28916				
CYS437	3.97987				
ILE115	4.76159				
ALA299	4.56472				
CYS437	4.4588				
ALA438	4.23068				
PHE430	4.85606				
Withaferin A					
GLN358	2.763	Hydrogen Bond	Conventional Hydrogen Bond	2013.02	-8.7
THR307	3.07606		Carbon Hydrogen Bond		
ILE115	4.49541	Hydrophobic	Alkyl		
LEU368	4.53714				
LEU368	4.88345				
VAL364	4.2692				
CYS437	3.74792				
ALA443	3.51861				
ALA299	4.99426				
ALA299	4.24537				
VAL364	4.15911				
CYS437	4.42435				
CYS437	4.89068				
ALA443	4.91757				
PHE207	4.82013		Pi-Alkyl		
PHE430	5.2985				
PHE430	4.48219				
PHE430	5.27249				
1,8-Cineole					

Amino Acid	Bond Length	Bond Type	Bond Category	Ligand Energy (Kcal/mol)	Docking Score
VAL364	4.48797	Hydrophobic	Alkyl	171.39	-6
LEU368	5.12235				
LEU368	5.23109				
LEU368	5.376				
PHE106	5.06353		Pi-Alkyl		
PHE116	5.10082				
PHE207	4.36329				
PHE298	4.96694				
PHE298	4.11652				
PHE298	4.95263				
PHE478	4.97142				
Curcumin					
LEU363	5.37325	Hydrophobic	Pi-Alkyl	211.18	-8.6
ALA443	4.95921				
VAL364	5.03313				
LEU368	4.95712				
Ferulic acid					
ILE115	2.49931	Hydrogen Bond	Conventional Hydrogen Bond	85.4	-8.1
TRP122	2.32165				
ARG126	2.32765				
ARG435	2.1098				
ARG435	1.87679				
GLY439	2.61659				
ILE115	4.38308	Hydrophobic	Pi-Alkyl		
ALA299	4.47908				
CYS437	4.63194				
ALA438	5.21682				
Cinnamaldehyde					
PHE430	4.19393	Hydrophobic	Pi-Pi Stacked	53.32	-6
LEU363	5.40575		Pi-Alkyl		
D-Mannose					
ALA443	4.70887	Hydrophobic	Pi-Alkyl	447.08	-5.8
Galangin					
GLN358	2.2687	Hydrogen Bond	Conventional Hydrogen Bond	180.12	-8.5
LEU363	1.98007				
LEU363	3.99629	Hydrophobic	Pi-Sigma		
LEU363	5.27835		Pi-Alkyl		
PRO429	4.98466				
VAL364	4.75363				
CYS437	4.28665				
Cinnamyl acetate					
PHE430	4.13663	Hydrophobic	Pi-Pi Stacked	66.32	-6.5
LEU363	5.41239		Pi-Alkyl		
6-Gingerol					
PHE298	3.93514	Hydrophobic	Pi-Sigma	111.63	-7
PHE430	4.6432		Pi-Pi T-shaped		
ALA299	4.15692		Alkyl		
LEU363	4.91772		Pi-Alkyl		
Shatavarin IV					
GLY300	1.90149	Hydrogen Bond	Conventional Hydrogen Bond	1031.47	-12.9
THR304	1.7047				
GLY439	2.84063				
ILE180	2.83175				
ALA299	3.51321		Carbon Hydrogen Bond		
GLY300	2.97167				
CYS437	3.83708	Hydrophobic	Alkyl		
ALA438	3.04738				
ILE115	4.3125				
VAL364	5.2595				
ILE115	4.44757				

Amino Acid	Bond Length	Bond Type	Bond Category	Ligand Energy (Kcal/mol)	Docking Score
ALA299	2.58894				
ILE115	4.69278				
LEU368	3.40836				
LEU210	4.6899				
ALA299	3.8526				
ALA299	3.26365				
ALA299	3.62996				
ALA299	4.76599				
VAL364	5.16739				
CYS437	4.08088				
CYS437	5.35871				
ALA438	4.06403				
PHE207	4.98573		Pi-Alkyl		
PHE478	3.79112				
Eugenol					
PHE430	4.48186	Hydrophobic	Pi-Pi Stacked	86.12	-6.6
LEU363	4.39616		Alkyl		
PRO429	4.55871				
ALA443	4.32663		Pi-Alkyl		
Costunolide					
ILE115	3.93095	Hydrophobic	Alkyl	322.63	-8
ALA299	3.81788				
VAL364	3.78935				
ILE115	5.17822				
LEU368	4.11519				
LEU368	4.6514				
PHE116	4.61616		Pi-Alkyl		
PHE207	4.29392				
Celapanine					
ARG100	2.54179	Hydrogen Bond	Conventional Hydrogen Bond	660.39	-6.5
ARG100	2.49275				
THR303	2.76482				
THR303	1.98649				
ALA299	3.01168		Carbon Hydrogen Bond		
LEU363	3.90032	Hydrophobic	Pi-Sigma		
PHE430	4.7835		Pi-Pi Stacked		
CYS437	4.15038		Alkyl		
ALA299	3.4422				
CYS437	4.40424				
VAL364	3.39327				
LEU368	4.05567				
CYS437	3.45639				
LEU368	5.02046				
VAL364	4.73604				
VAL364	5.37681				
CYS437	5.03916				
CYS437	3.76052				
PHE116	5.47149		Pi-Alkyl		
PHE298	5.3469				
PHE430	4.01154				
Purpurin					
ASN367	2.34989	Hydrogen Bond	Conventional Hydrogen Bond	150.14	-8
ALA438	2.97709		Pi-Donor Hydrogen Bond		
ALA438	3.20896				
LEU368	3.84177	Hydrophobic	Pi-Sigma		
ALA438	3.78661				
CYS437	4.19358		Pi-Alkyl		
ILE115	4.77011				
ALA299	5.19197				

Amino Acid	Bond Length	Bond Type	Bond Category	Ligand Energy (Kcal/mol)	Docking Score
CYS437	4.32892				
ALA438	4.9686				
ILE114	5.10209				
ILE115	4.35288				
ALA299	4.42706				
Juglone					
THR303	2.32943	Hydrogen Bond	Conventional Hydrogen Bond	87.58	-7.2
THR304	3.04577				
PHE430	4.53603	Hydrophobic	Pi-Pi Stacked		
PHE430	4.18035				
ALA443	4.29293		Pi-Alkyl		
CYS437	5.19156				
Amygdalin					
PRO429	2.02457	Hydrogen Bond	Conventional Hydrogen Bond	1399.48	-10.2
PRO429	2.61757				
ASN367	2.3114				
ARG435	2.16405				
ARG126	2.68298				
ARG126	2.62563				
ALA438	2.97374		Pi-Donor Hydrogen Bond		
ALA438	3.60801	Hydrophobic	Pi-Sigma		
CYS437	4.96956	Other	Pi-Sulfur		
LEU368	5.25271	Hydrophobic	Pi-Alkyl		
CYS437	3.83479				
LEU363	4.99903				
ILE115	4.95182				
ALA299	4.10633				
Lauric acid					
PHE298	2.3176	Hydrogen Bond	Conventional Hydrogen Bond	3.94	-5.8
THR303	2.20862				
THR303	1.98314				
VAL364	3.76101	Hydrophobic	Alkyl		
LEU368	5.31181				
PHE207	5.01311		Pi-Alkyl		
Sarsasapogenin					
ILE114	2.52415	Hydrogen Bond	Conventional Hydrogen Bond	792.54	-4.2
ILE115	2.81216				
LEU368	4.33109	Hydrophobic	Alkyl		
LEU363	4.51188				
CYS437	4.34245				
VAL364	3.34281				
LEU368	4.9397				
VAL364	3.70899				
ILE361	5.25402				
LEU363	4.06726				
ILE115	5.00423				
ALA299	5.09617				
VAL364	5.24066				
CYS437	4.0772				
CYS437	3.81462				
CYS437	3.73757				
ALA438	5.35926				
PHE430	5.4535		Pi-Alkyl		
PHE430	4.90055				
Aloe-emodin					
ILE115	2.86127	Hydrogen Bond	Conventional Hydrogen Bond	153.88	-8.3
CYS437	2.98644				
ARG100	2.59577				
ARG435	1.95894				
LEU368	3.792	Hydrophobic	Pi-Sigma		

Amino Acid	Bond Length	Bond Type	Bond Category	Ligand Energy (Kcal/mol)	Docking Score
PHE430	5.02613		Amide-Pi Stacked		
ILE115	4.56353		Pi-Alkyl		
CYS437	5.46059				
CYS437	4.26494				
VAL364	4.71288				
LEU368	5.18264				
CYS437	4.40794				
Caffeic acid					
PRO429	2.51051	Hydrogen Bond	Conventional Hydrogen Bond	59.2	-6.9
LEU363	1.99381				
VAL364	2.28551				
ALA443	4.42848	Hydrophobic	Pi-Alkyl		
LEU447	5.38973				

Table 3. 2D and 3D binding interaction profiles of selected phytochemicals and the native ligand within the active site of CYP2E1, illustrating key molecular interactions and binding conformations.

3D Binding Interaction Pose	2D Binding Interaction Pose
Native Ligand	
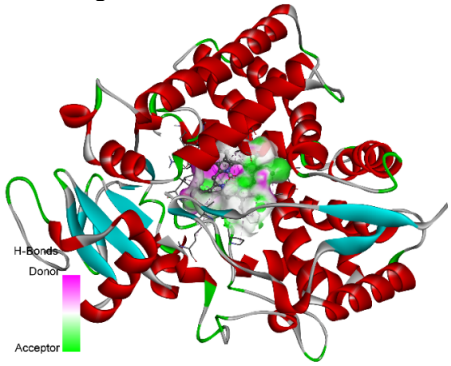	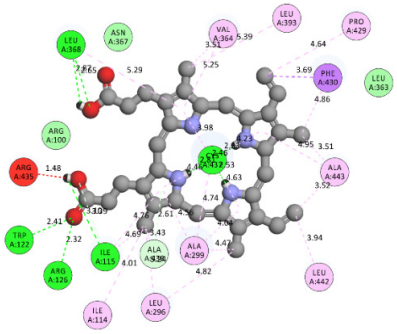
Withaferin A	
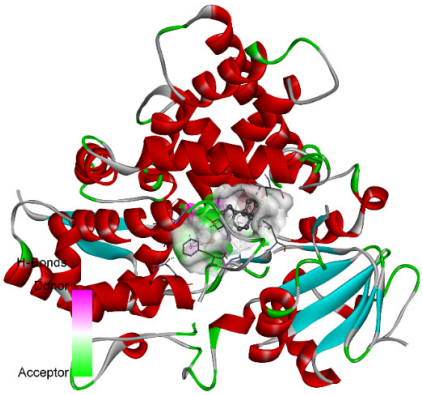	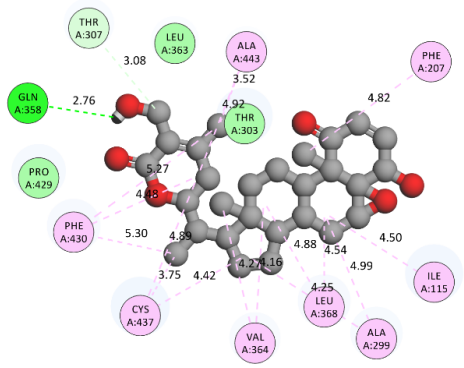
1,8-Cineole (Eucalyptol)	
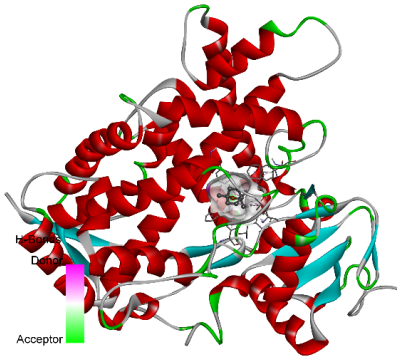	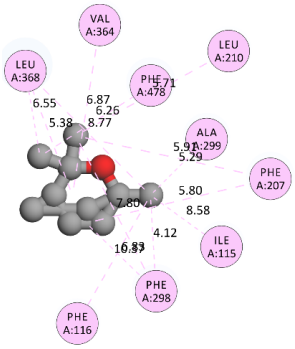

3D Binding Interaction Pose	2D Binding Interaction Pose
Curcumin	
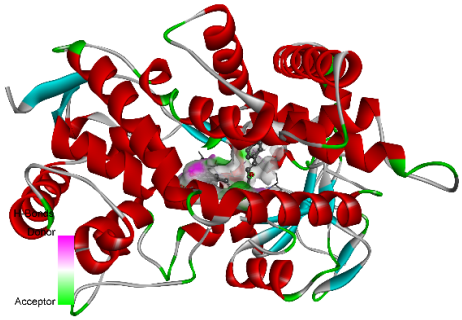	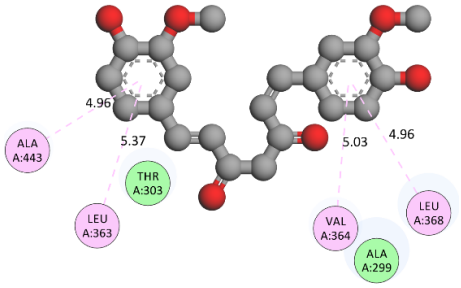
Ferulic acid	
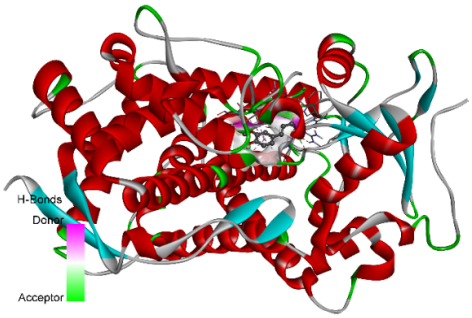	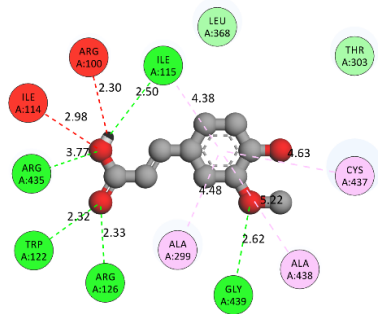
Cinnamaldehyde	
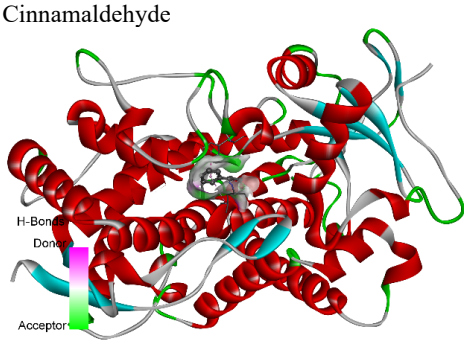	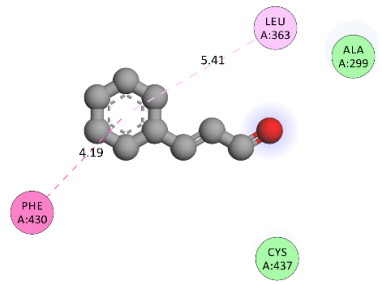
D-Mannose	
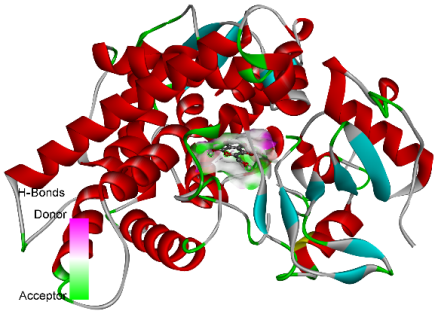	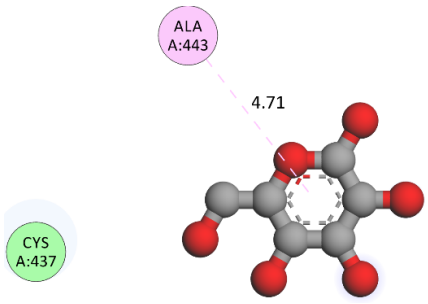
Galangin	
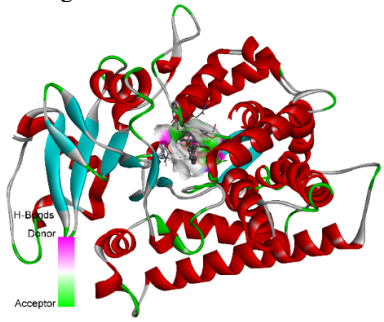	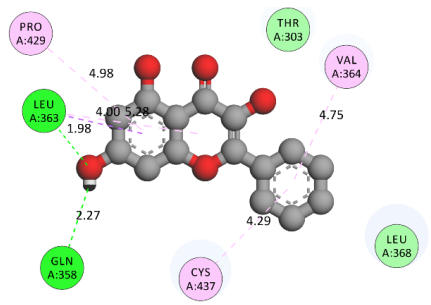

3D Binding Interaction Pose	2D Binding Interaction Pose
Cinnamyl acetate	
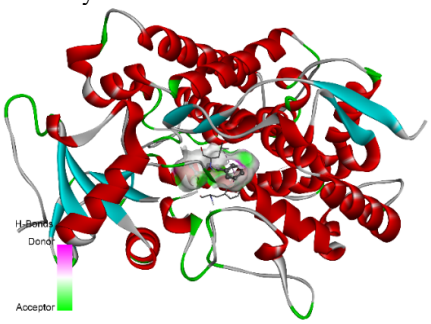	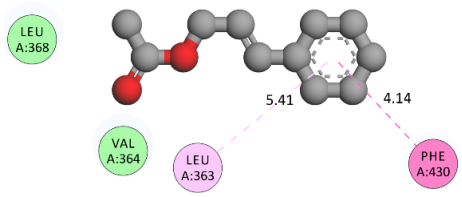
6-Gingerol	
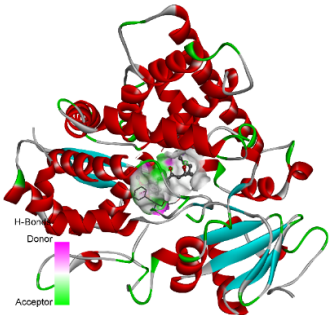	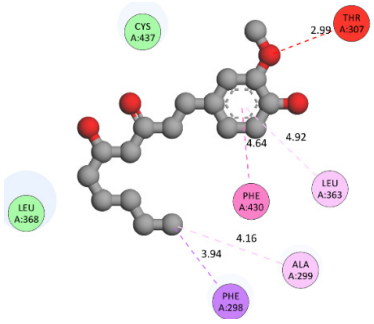
Shatavarin IV	
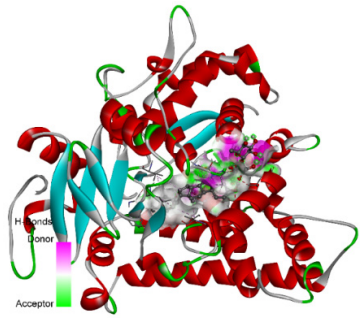	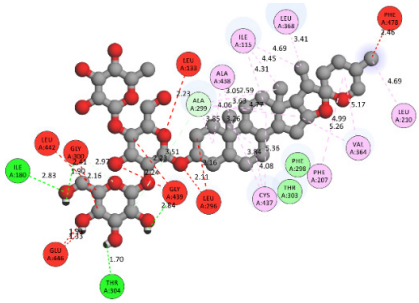
Eugenol	
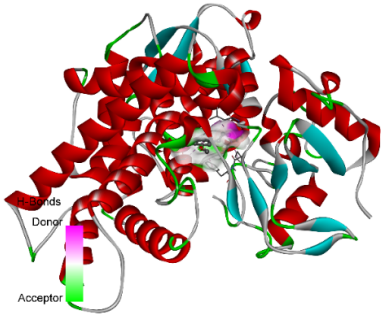	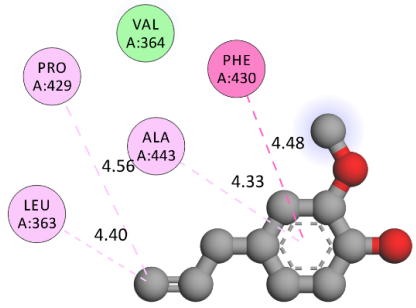
Costunolide	
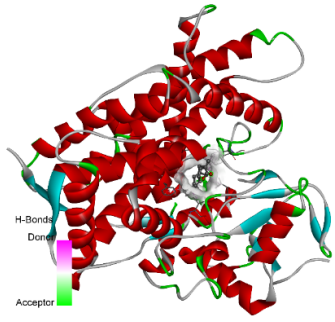	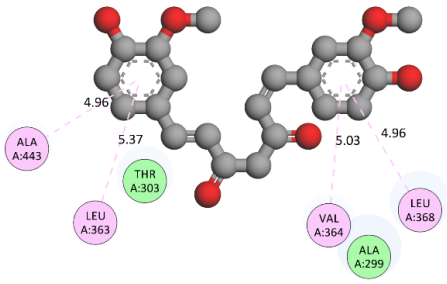

3D Binding Interaction Pose	2D Binding Interaction Pose

Celapanine

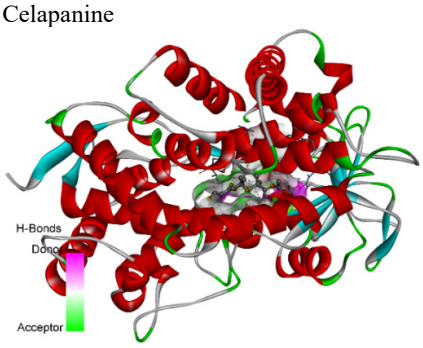

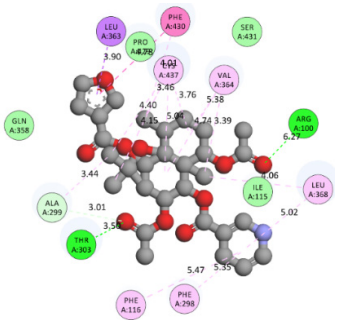

Purpurin

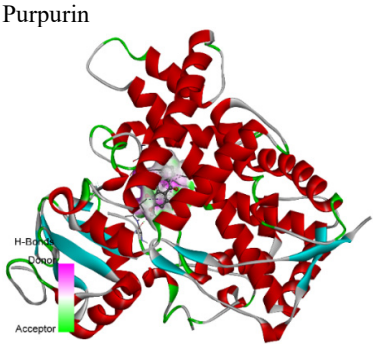

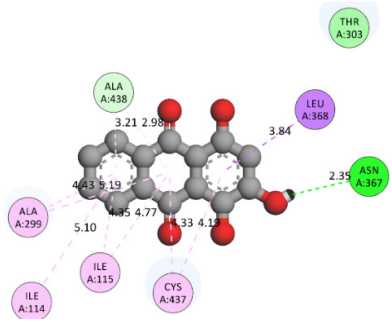

Juglone

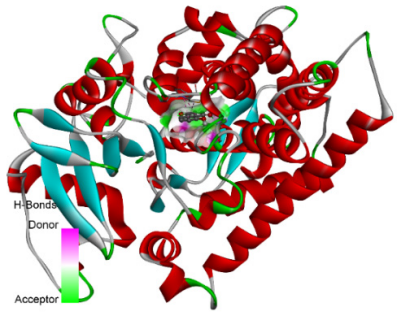

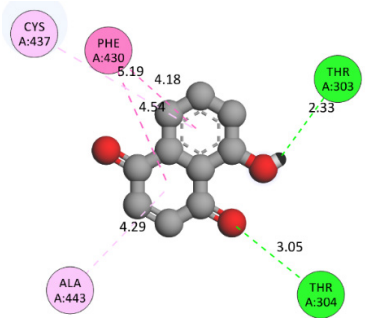

Amygdalin

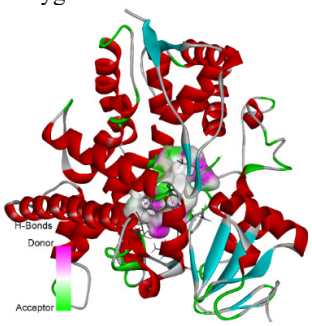

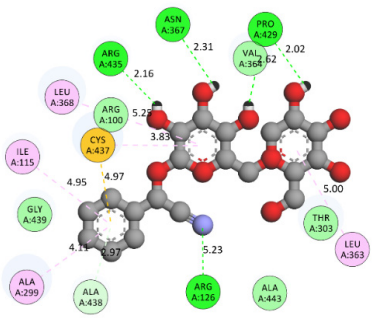

Lauric acid

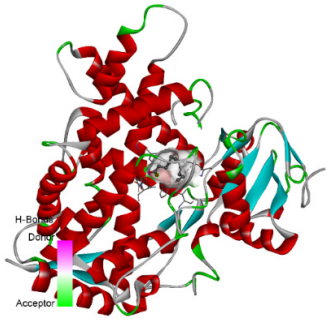

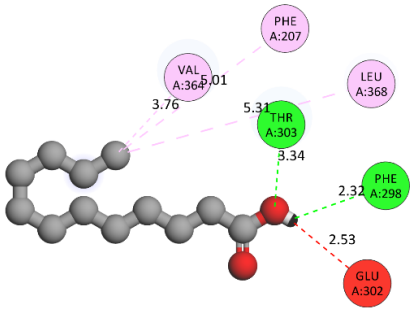

3D Binding Interaction Pose	2D Binding Interaction Pose
Sarsasapogenin	
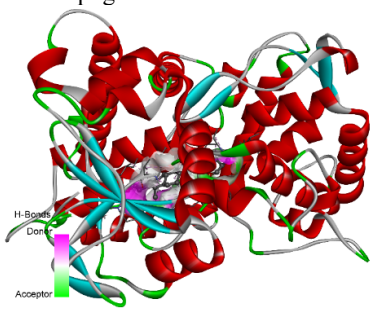	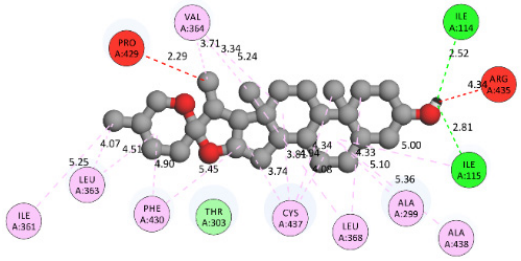
Aloe-emodin	
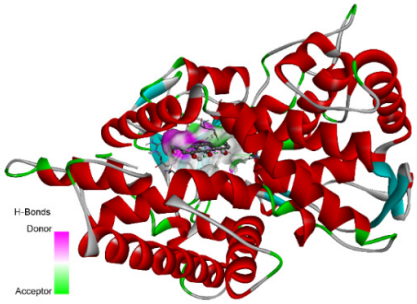	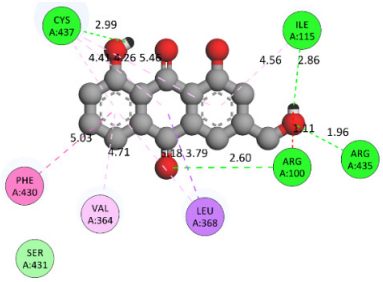
Caffeic acid	
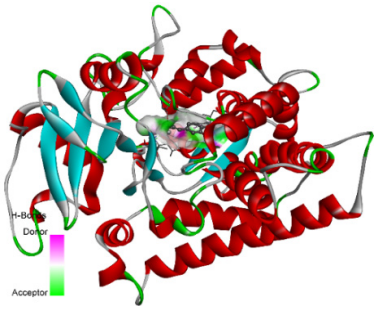	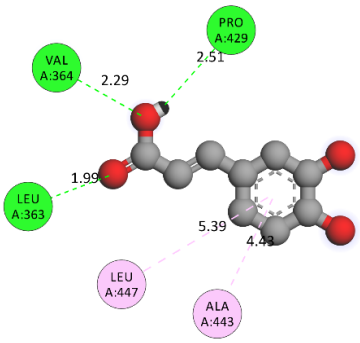

3.2. ADMET analysis

Based on the molecular docking results, nine top-performing phytochemicals—Withaferin A, Curcumin, Ferulic acid, Galangin, Shatavarin IV, Costunolide, Purpurin, Amygdalin, and Aloe-emodin—were selected as the most potent compounds because of their superior binding affinities and stable interactions within the active site of CYP2E1. These compounds exhibited comparable or improved interaction patterns relative to the native ligand, particularly involving key catalytic residues. Consequently, these nine shortlisted candidates, along with the native ligand as a reference standard, were subjected to comprehensive ADMET evaluation to assess their pharmacokinetic behavior, drug-likeness, safety profiles, and environmental impacts. ADMET evaluation was conducted to systematically analyze the absorption, distribution, metabolism, excretion, toxicity, and environmental parameters of the selected potent compounds in comparison with those of the native ligand. A detailed interpretation of each dataset (Tables 1–6) provides deeper insights into their suitability and prioritization as potential drug candidates. As presented in Table 4, the native ligand possesses a relatively high molecular weight (562.26 g/mol), elevated TPSA (131.96 Å²), and moderate lipophilicity (LogP 3.29), suggesting acceptable membrane permeability but potential limitations in oral bioavailability due to its size and polarity. In comparison, several phytochemicals have demonstrated more favorable physicochemical characteristics. Ferulic acid exhibited the most optimal profile, with a low molecular weight (194.06 g/mol), moderate TPSA (66.76 Å²), and balanced lipophilicity (logP 1.64), indicating improved permeability and solubility compared to the native ligand. Curcumin, Galangin, Aloe-emodin, and Costunolide also fell within the acceptable drug-like space, showing lower molecular weights and manageable hydrogen bonding capacities. Conversely, Shatavarin IV (MW 886.49 g/mol; TPSA 255.91 Å²) and amygdalin (TPSA 202.32 Å²; 12 HBA, 7 HBD) displayed excessive polarity and hydrogen bonding potential, which may negatively influence

membrane permeability and oral absorption. Overall, Ferulic acid, Curcumin, Galangin, and Aloe-emodin demonstrated a more favorable physicochemical balance than the native ligand. As shown in Table 5, the native ligand exhibited a low QED score (0.225), indicating moderate overall drug-likeness properties. In contrast, several phytochemicals showed significantly improved QED values, particularly ferulic acid (0.715), galangin (0.632), aloe-emodin (0.62), and curcumin (0.548), indicating stronger compliance with the drug-like chemical space. These compounds also satisfied major medicinal chemistry filters, such as Lipinski, Pfizer, GSK, and Golden Triangle rules, more effectively than the native ligand. Shatavarin IV and Amygdalin showed one Lipinski violation each, largely due to their high molecular weight and excessive hydrogen bond donors/acceptors, which may compromise oral bioavailability. Costunolide and Withaferin A exhibited moderate QED values but favorable natural product (NP) scores, indicating promising structural diversity. Overall, Ferulic acid and aloe-emodin demonstrated superior drug-likeness profiles relative to the native ligand, suggesting better development potential. The absorption data summarized in Table 6 reveal that the native ligand has poor Caco-2 permeability (− 5.8075) and extremely low HIA probability (7.15E-07), indicating limited intestinal absorption and potentially low oral bioavailability. In comparison, ferulic acid (HIA 0.24942), aloe-emodin (0.32913), and costunolide (0.15512) exhibited significantly improved intestinal absorption potential. Curcumin demonstrated an excellent predicted fraction absorbed (F50% 0.99945), supporting its strong oral absorption capability. Despite its strong docking performance, Shatavarin IV displayed poor Caco-2 permeability (–6.2296) and high P-gp substrate probability (0.61915), suggesting potential efflux issues and reduced systemic exposure. Amygdalin also exhibited moderate permeability limitations. Galangin exhibited moderate probability of P-gp inhibition, which may influence transport dynamics. Overall, Ferulic acid, Curcumin, and Aloe-emodin demonstrated markedly improved absorption properties compared to the native ligands. As shown in Table 7, the native ligand displayed very high plasma protein binding (98.90%), which may significantly reduce free drug concentration in systemic circulation. Curcumin and Galangin also exhibited similarly high PPB values (>97%), while Ferulic acid (68.60%) and Shatavarin IV (59.72%) demonstrated comparatively lower PPB, potentially increasing their free fraction and therapeutic availability. Regarding metabolic stability, the native ligand showed high CYP2D6 substrate probability, indicating susceptibility to rapid metabolism and possible drug–drug interactions. Curcumin and Galangin interacted with multiple CYP isoforms, suggesting higher metabolic liability. In contrast, Shatavarin IV exhibited minimal CYP inhibition probabilities, indicating lower risk of metabolic interference. Ferulic acid also showed relatively limited CYP interactions, supporting a safer metabolic profile. Therefore, Ferulic acid and Shatavarin IV presented improved metabolic safety compared to the native ligand.

Table 4. Physicochemical properties of selected derivatives

Compounds	MW	Volume	Dense	nHA	nHD	nRot	nRing	TPSA	logS	logP
Native Ligand	562.26	593.439	0.94746	8	4	8	5	131.96	-3.9103	3.29366
Withaferin A	470.27	483.701	0.97223	6	2	3	6	96.36	-4.1887	2.923
Curcumin	368.13	381.036	0.96613	6	2	8	2	93.06	-3.6199	2.1471
Ferulic acid	194.06	194.938	0.99549	4	2	3	1	66.76	-2.3639	1.64768
Galangin	270.05	265.186	1.01834	5	3	1	3	90.9	-3.1956	2.22534
Shatavarin IV	886.49	859.302	1.03164	17	9	8	9	255.91	-4.872	1.89916
Costunolide	232.15	257.918	0.90009	2	0	0	2	26.3	-3.237	2.92294
Purpurin	256.04	247.89	1.03288	5	3	0	3	94.83	-5.0418	2.92342
Amygdalin	457.16	423.314	1.07996	12	7	7	3	202.32	-1.3306	-0.6597
Aloe-emodin	270.05	265.186	1.01834	5	3	1	3	94.83	-5.4275	2.94029

Table 5. Drug-likeness properties of designed derivatives

Compounds	QED	NP Score	Lipinski Rule	Pfizer Rule	GSK Rule	Golden Triangle	Chelator Rule
Native Ligand	0.225	0.647	0	0	1	1	0
Withaferin A	0.485	3.881	0	0	1	0	0
Curcumin	0.548	0.722	0	0	0	0	1
Ferulic acid	0.715	0.926	0	0	0	1	1
Galangin	0.632	1.429	0	0	0	0	1
Shatavarin IV	0.149	2.379	1	0	1	1	0
Costunolide	0.363	3.385	0	0	0	0	0
Purpurin	0.419	1.124	0	0	0	0	1
Amygdalin	0.218	1.212	1	0	1	0	0
Aloe-emodin	0.62	1.356	0	0	0	0	0

Table 6. Absorption parameters of selected compounds

Compounds	Caco-2 Permeability	MDCK Permeability	Pgp-inhibitor	Pgp-substrate	HIA	F20%	F30%	F50%
Native Ligand	-5.8075	-5.2991	4.02E-06	0.00217	7.15E-07	6.54E-05	9.18E-06	0.05742
Withaferin A	-5.2666	-5.0035	0.10658	0.00272	0.00128	0.00729	0.49401	0.93853
Curcumin	-5.4714	-4.9408	0.27956	0.00917	0.01711	0.78524	0.47893	0.99945
Ferulic acid	-4.9886	-4.7914	0.00451	0.05045	0.24942	0.95667	0.93298	0.99327
Galangin	-5.3527	-4.8325	0.90889	0.10163	0.01689	0.01421	0.75177	0.93348
Shatavarin IV	-6.2296	-4.9468	0.00086	0.61915	0.00132	0.07506	0.97784	0.9976
Costunolide	-4.7741	-4.6164	0.98927	0.01298	0.15512	0.13227	0.46441	0.62761
Purpurin	-4.9795	-4.7533	0.88213	0.02523	0.10652	0.03774	0.93732	0.99031
Amygdalin	-5.4452	-4.7561	0.00012	0.31513	0.13851	0.00439	0.98616	0.72239
Aloe-emodin	-5.0622	-4.6877	0.07149	0.05061	0.32913	0.09768	0.97688	0.98523

Table 7. Distribution and metabolism parameters of selected molecules

Compounds	Distribution				Metabolism									
					CYP1A2		CYP2C19		CYP2C9		CYP2D6		CYP3A4	
	PPB %	VD	BBB	Fu	Inhibitor	Substrate	Inhibitor	Substrate	Inhibitor	Substrate	Inhibitor	Substrate	Inhibitor	Substrate
Native Ligand	98.9005	-0.163	4.40E-05	0.62088	1	3.33E-05	0.22316	0.00021	5.05E-06	0.9992	0.00116	1.52E-05	1.63E-08	1.14E-08
Withaferin A	77.8184	-0.14	0.01258	17.4918	1.89E-05	0.01639	2.71E-07	0.68609	1.90E-07	0.00185	5.66E-05	0.03066	3.74E-07	0.17189
Curcumin	97.0507	-0.6981	0.02254	2.00245	0.99583	0.00017	0.49062	0.00429	0.26905	0.00592	0.01801	0.88862	0.01427	0.0001
Ferulic acid	68.6005	-0.7268	0.00113	25.1921	0.01832	0.00027	0.00078	0.01618	0.01841	0.13468	0.00113	0.01611	0.00035	0.00022
Galangin	98.1731	-0.5201	0.02298	0.68853	0.99671	0.45725	0.39696	0.00081	0.92819	0.97203	0.02441	0.99492	0.132	0.001
Shatavarin IV	59.7233	-0.3807	0.00206	30.7441	1.06E-11	5.72E-10	2.24E-09	0.0013	1.15E-07	5.20E-12	5.05E-07	4.82E-11	1.14E-05	0.99645
Costunolide	95.9796	0.09802	0.00333	4.36461	0.60539	0.25093	0.13735	0.59602	0.03845	0.89782	0.08128	0.60674	0.20579	0.08804
Purpurin	95.7177	0.30828	0.00289	5.33496	0.99638	0.99057	0.00103	0.00208	0.00419	0.00994	0.00071	5.04E-05	0.00633	0.00015
Amygdalin	61.7035	-0.576	0.00119	43.6245	2.22E-10	0.00064	1.25E-08	0.00017	3.65E-06	1.24E-07	2.02E-08	3.14E-11	8.84E-06	0.00377
Aloe-emodin	92.3123	0.86631	0.00018	10.4407	0.09511	0.06321	0.31568	0.72515	0.04356	0.00115	0.00181	5.06E-05	0.00017	0.47018

The excretion and toxicity results in Table 8 indicate that the native ligand has moderate clearance (0.85679) but a very high DILI probability (0.97358), suggesting a potential hepatotoxicity risk. In contrast, curcumin (DILI 0.03264) and Withaferin A (0.17684) demonstrated substantially lower hepatotoxicity probabilities, indicating improved hepatic safety. Shatavarin IV and Amygdalin showed longer half-lives (>3 h), suggesting sustained systemic presence, although prolonged exposure may increase toxicity concerns. Purpurin and Aloe-emodin exhibited higher Ames toxicity probabilities, indicating a possible risk of mutagenicity. Ferulic acid demonstrated moderate safety, with relatively balanced toxicity indicators. Compared with the native ligands, Curcumin and Withaferin A showed superior safety profiles, whereas ferulic acid maintained acceptable toxicity characteristics.

The environmental toxicity parameters shown in Table 9 reveal a moderate bioaccumulation potential for the native ligand (BCF 0.42233). Costunolide (BCF

2.2263) and Shatavarin IV (1.80627) exhibited higher bioaccumulation tendencies, suggesting potential environmental persistence. Ferulic acid showed the lowest BCF value (0.18364), indicating a minimal bioaccumulation risk. Similarly, Ferulic acid displayed lower aquatic toxicity indicators (IGC50, LC50FM, LC50DM) than several other compounds. Curcumin and Aloe-emodin exhibited moderate environmental profiles, whereas costunolide exhibited comparatively higher toxicity values. Overall, Ferulic acid demonstrated the safest environmental toxicity profile among the tested compounds and was comparatively more favorable than the native ligand.

As shown in Tables 4–9, ferulic acid consistently demonstrated the most balanced ADMET profile compared to the native ligand, followed by Curcumin and Aloe-emodin. Withaferin A showed reduced hepatotoxicity risk, whereas Shatavarin IV exhibited strong metabolic stability but poor absorption due to its high molecular weight and polarity. Collectively, these findings suggest that ferulic acid, Curcumin, Aloe-emodin, and Withaferin A exhibit improved pharmacokinetic and safety profiles relative to the native ligands, supporting their potential for further development. The ADMET radar of the potent compounds is shown in Table 10.

Table 8. Excretion and Toxicity parameters of selected compounds

Compounds	Excretion		Toxicity									
	CL-plasma	T1/2	H-HT	DILI	Ames Toxicity	Rat Oral Acute Toxicity	FDAMDD	Skin Sensitization	Carcinogenicity	Eye Corrosion	Eye Irritation	Respiratory Toxicity
Native Ligand	0.85679	1.4398	0.63568	0.97358	0.22828	0.4906	0.82889	0.30861	0.35416	8.62E-06	0.90115	0.98191
Withaferin A	9.07905	1.40503	0.38638	0.17684	0.49473	0.24431	0.62769	0.99551	0.95611	0.05092	0.83782	0.72764
Curcumin	8.52212	1.04041	0.42901	0.03264	0.29299	0.09186	0.30271	0.99467	0.13789	0.13153	0.95886	0.76245
Ferulic acid	8.35884	1.6978	0.70188	0.63561	0.25205	0.081	0.19426	0.743	0.24897	0.76117	0.99663	0.60786
Galangin	4.63486	1.05168	0.41885	0.84676	0.5599	0.50762	0.75499	0.57632	0.70554	0.59239	0.99668	0.72056
Shatavarin IV	0.14812	3.29083	0.54497	0.96012	0.84069	0.00394	0.00467	1	0.05511	1.96E-07	0.00095	0.00028
Costunolide	9.4869	1.83564	0.73692	0.93913	0.54245	0.24269	0.40858	0.98427	0.6496	0.49387	0.97722	0.25555
Purpurin	6.33326	2.00739	0.65277	0.91575	0.91452	0.52037	0.33004	0.96273	0.86462	0.02374	0.99324	0.82357
Amygdalin	1.34535	3.52932	0.63314	0.9258	0.88843	0.05381	0.03206	0.99953	0.00618	1.70E-05	0.29417	0.07692
Aloe-emodin	4.80549	1.20219	0.67982	0.90649	0.92301	0.35846	0.31187	0.88418	0.83197	0.00016	0.9711	0.86906

Table 9. Environmental toxicity profile of designed molecules

Compounds	BCF	IGC50	LC50FM	LC50DM
Native Ligand	0.42233	3.24718	3.81702	4.62519
Withaferin A	1.32264	4.01817	5.12274	5.84702
Curcumin	0.81551	3.59024	4.19259	4.58036
Ferulic acid	0.18364	2.7564	3.23844	3.97939
Galangin	1.15481	4.09904	4.53145	4.84314
Shatavarin IV	1.80627	3.45121	4.01484	4.60404
Costunolide	2.2263	4.49433	5.64602	6.03023
Purpurin	1.62815	4.25969	4.66394	5.10762
Amygdalin	0.44297	2.77898	3.33516	4.59004
Aloe-emodin	1.43412	3.54384	3.96287	4.82318

Table 10. ADMET radar of the most potent compounds and native ligand

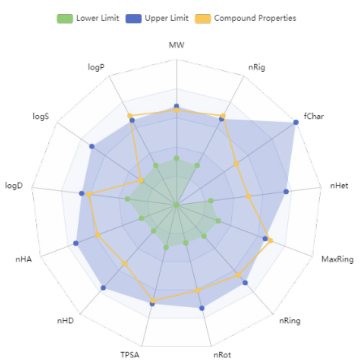

Native Ligand

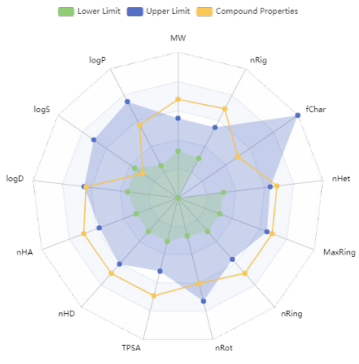

Shatavarin IV

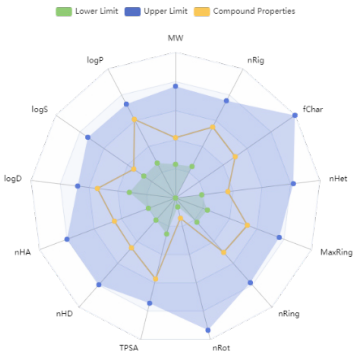

Galangin

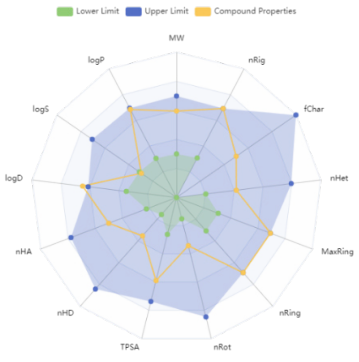

Withaferin A

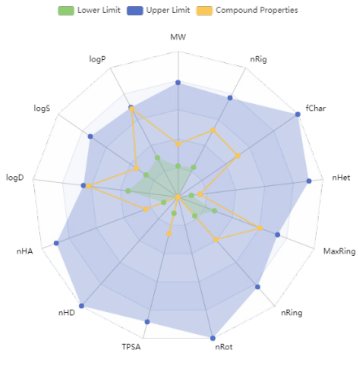

Costunolide

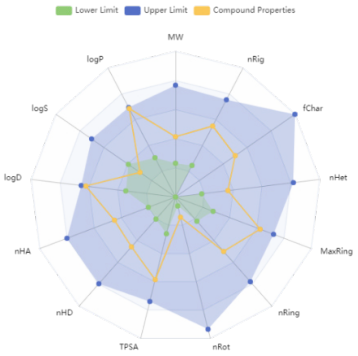

Aloe-emodin

Curcumin

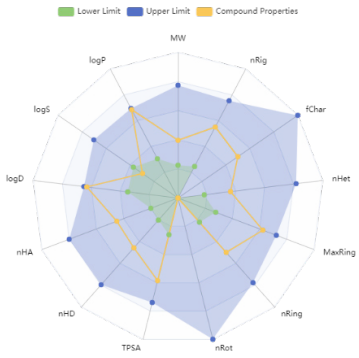

Purpurin

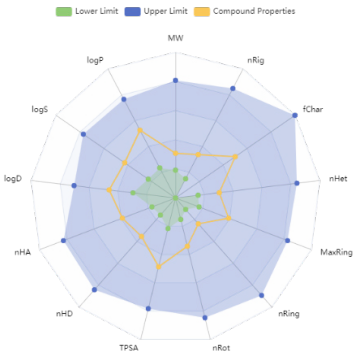

Ferulic acid

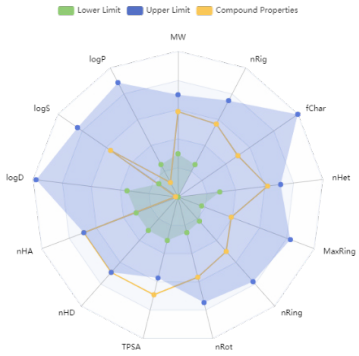

Amygdalin

4. Conclusion

In conclusion, the present study integrated molecular docking and comprehensive ADMET analysis to identify potential CYP2E1-interacting phytochemicals using a computational screening approach. The docking results demonstrated that several phytochemicals effectively occupied the catalytic pocket and interacted with key residues, such as CYS437, ILE115, LEU368, ALA299, VAL364, and PHE430, similar to the native ligand. Shatavarin IV exhibited the strongest binding affinity, surpassing that of the native ligand, with multiple hydrogen bonds and hydrophobic interactions, suggesting favorable ligand–protein interactions within the predicted binding site. Amygdalin also showed a strong binding affinity, whereas Withaferin A, Curcumin, Galangin, Aloe-emodin, and Ferulic acid demonstrated moderate yet significant interactions within the active site. However, ADMET evaluation highlighted important pharmacokinetic differences. Although Shatavarin IV showed superior docking performance, its high molecular weight and elevated TPSA suggest poor absorption potential. In contrast, ferulic acid, Curcumin, and Aloe-emodin exhibited balanced physicochemical properties, improved intestinal absorption, acceptable metabolic profiles, and comparatively lower toxicity risks than native ligands. Ferulic acid, in particular, demonstrated the most favorable overall ADMET and environmental safety profiles. Based on the combined interpretation of the docking and ADMET results, ferulic acid, Curcumin, Aloe-emodin, and Withaferin A were identified as promising candidates for further investigation. However, the findings of this study are based solely on computational predictions and should be considered preliminary. Therefore, molecular dynamics simulations, in vitro CYP2E1 inhibition assays, and in vivo studies are required to validate the predicted binding behavior, pharmacological activity, and safety profiles of these phytochemicals before any definitive conclusions regarding their therapeutic potential can be drawn.

References

[1] Li Y, Hong X, Liang L, Wang X, Ladd-Acosta C. Association between acetaminophen metabolites and CYP2E1 DNA methylation level in neonate cord blood in the Boston Birth Cohort. Clin Epigenetics. 2023;15(1).

[2] Zhu L, Yang X, Feng J, Mao J, Zhang Q, He M, et al. CYP2E1 plays a suppressive role in hepatocellular carcinoma by regulating Wnt/Dvl2/β-catenin signaling. J Transl Med. 2022;20(1).

[3] Wang K, Tan W, Liu X, Deng L, Huang L, Wang X, et al. New insight and potential therapy for NAFLD: CYP2E1 and flavonoids. Biomed Pharmacother. 2021;137.

[4] Cawley GF, Connick JP, Eyer MK, Backes WL. Environmentally persistent free radicals stimulate CYP2E1-mediated generation of reactive oxygen species at the expense of substrate metabolism. Drug Metab Dispos. 2025;53(1).

[5] Wang Y, Chen Q, Wu S, Sun X, Yin R, Ouyang Z, et al. Amelioration of ethanol-induced oxidative stress and alcoholic liver disease by in vivo RNAi targeting Cyp2e1. Acta Pharm Sin B. 2023;13(9):3906-18.

[6] (a) Singla RK, Wang X, Gundamaraju R, Joon S, Tsagkaris C, Behzad S, et al. Natural products derived from medicinal plants and microbes might act as a game-changer in breast cancer: a comprehensive review of preclinical and clinical studies. Crit Rev Food Sci Nutr. 2023;63(33):11880-924. (b) Jiang M, Wang T, Simal-Gandara J, Nayaka Siddaiah C, Dai XF, Chen JY, et al. Overview of the control of plant fungal pathogens by natural products derived from medicinal plants. Plant Prot Sci. 2023;59(4):303-16.

[7] Ahmed AA, Mohammed MA. Analytical, chemical, and biological perspectives on quercetin: structure, biosynthesis, extraction methods, and metal complexation—a review. Anal Methods Environ Chem J. 2026;9(2):98-121. https://doi.org/10.24200/amecj.v9.i02.1114

[8] Elsherif KM, Sulaiman MA, Mlitan AM. Ruta graveolens L. leaves as a potential source of natural antioxidants and phytochemicals: a study from Msallata, Libya. Chem Res Technol. 2026;3(1):28-36. https://doi.org/10.22034/chemrestec.2025.558398.1072

[9] (a) Philbin CS, Dyer LA, Jeffrey CS, Glassmire AE, Richards LA. Structural and compositional dimensions of phytochemical diversity in the genus Piper reflect distinct ecological modes of action. J Ecol. 2022;110(1):57-67. (b) Lahrizi L, Errachidi F, Nekhla H, El Ghadraoui L. Ajuga iva L.: an overview of phytochemical profile and biological functionalities. Chem Rev Lett. 2024;7(1):31-44. https://doi.org/10.22034/crl.2024.413946.1241 (c) Venugopala KN. Flavonoids as multifunctional phytochemicals: structural diversity, pharmacological potential and therapeutic prospects. Asian J Chem. 2025;37(12):2947-62.

[10] (a) Soleimani-Amiri S, Mohammadi M, Faal Hamedani N, Dehbandi B. An efficient synthesis and study of biological activity of new pyrimidoazepines using Ag/Fe3O4/TiO2/CuO@MWCNTs magnetic nanocomposites: a combined experimental and theoretical investigation. Polycycl Aromat Compd. 2023;43(7):6046-6075. https://doi.org/10.1080/10406638.2022.2112709 (b) Soleimani-Amiri S, Koohi M. (E)-3-X-indoline-2-ones as potent and selective inhibitors against different receptor tyrosine kinase (RTKs) in solution vs gas phase, at DFT. J Phys Org Chem. 2019;32:e3929. https://doi.org/10.1002/poc.3929 (c) Radhi IJ, Abdul Amir IQ, Shaker ZM, Soleimani-Amiri S, Imanov HA, Khanmohammadi A, et al. DFT investigation of 5-fluorouracil adsorption on Fe/Mg–N_4 carbon coordination frameworks: mechanistic insights. J Saudi Chem Soc. 2026;30(3):36. https://doi.org/10.1007/s44442-026-00086-6 (d) Al-Sultan SQ, Mohammed MH, Talib WH. Newly designed 2-(aminomethyl)benzimidazole derivatives as possible tyrosine kinase inhibitors: synthesis, characterization, preliminary cytotoxic evaluation and in silico studies. Chem Rev Lett. 2024;7(3):545-559. https://doi.org/10.22034/crl.2024.463505.1360

[11] (a) Khan SL, Sonwane GM, Siddiqui FA, Jain SP, Kale MA, Borkar VS. Discovery of naturally occurring flavonoids as human cytochrome P450 (CYP3A4) inhibitors with the aid of computational chemistry. Indo Glob J Pharm Sci. 2020;10(04):58-69. (b) El Jabboury Z, Aazza S, OUSAAID D, Lahrizi L, El Kamari F, Benjelloun M, et al. Comprehensive analysis of phytochemistry, in silico toxicity prediction, and antimicrobial efficacy across different fractions of Ammi visnaga L. Chem Rev Lett. 2024;7(2):359-372. https://doi.org/10.22034/crl.2024.429586.1267 (c) Badawy MAS, Bräse S, Ali TFS, Abdel-Aziz M, Abdel-Rahman HM. Biologically active benzimidazole hybrids as cancer therapeutics: recent advances. Pharmaceuticals. 2025;18(10).

[12] (a) Yakubu J, Gimba FM, Muhammed A, Maikau FU, Tanko U, Ibrahim S. Nutritional, phytochemical, and antimicrobial study of Ocimum basilicum methanolic leaf extract. J Med Med Chem. 2025;7(3):66-72. (b) Muhammed A, Yakubu J, Maikau FU, Gimba FM, Tanko U, Ibrahim S. Phytochemical screening, isolation, characterization and antimicrobial evaluation of Syzygium cumini leaf extracts. J Chem Technol. 2026;2(1):17-25. (c) Muhee AA, Kadhim MI. Synthesis, antibacterial and molecular docking of some new tetrazole, oxazepine and thiazolidine derivatives contacting with aromatic nucleus. Chem Rev Lett. 2024;7(4):647-654. https://doi.org/10.22034/crl.2024.459423.1341

[13] (a) Al-Gburi K, Naser NH, Jasamai M. Searching for newer histone deacetylase 6 inhibitors: design, ADMET prediction, molecular docking, and molecular dynamics simulation of new isatin hydrazones. Chem Rev Lett. 2026;9(1):98-112. https://doi.org/10.22034/crl.2025.517272.1583 (b) Kayyal M, Olyaei A, Pourshamsian K, Sadeghpour M. Molecular docking and prediction of ADME/drug-likeness properties of some benzochromenopyrimidine derivatives as inhibitors of cyclooxygenase-2 (COX-2). Chem Rev Lett. 2025;8(2):300-308. https://doi.org/10.22034/crl.2024.483994.1453 (c) Roney M, Aluwi MFFM. Anti-diabetic activity of phloretin against maltase-glucoamylase using docking, pharmacokinetics and pharmacophore studies. J Chem Lett. 2023;4(3):164-170. https://doi.org/10.22034/jchemlett.2023.411216.1131 (d) Isa AS, Mohammed AM. Computational analysis of novel 4-thiazolidinone derivatives as potential anti-breast cancer agents: docking, pharmacokinetics, and molecular dynamics study. Med Med Chem. 2024;1(3):102-114. https://doi.org/10.22034/medmedchem.2024.488996.1015 (e) Amos-Tautua BM, Ajoko IT, Oyaseiye PE, Overe R. Computational screening and ADMET assessment of leaf extracts of Anthocleista djalonensis and Funtumia africana targeting tumor necrosis factor-alpha enzyme. J Med Chem. 2026;2(1):43-55. https://doi.org/10.22034/jmedchem.2026.576002.1031

[14] Dutta R, Khalil R, Green R, Mohapatra SS, Mohapatra S. Withania somnifera (Ashwagandha) and withaferin A: potential in integrative oncology. Int J Mol Sci. 2019;20.

[15] Pavarino M, Marengo A, Cagliero C, Bicchi C, Rubiolo P, Sgorbini B. Elettaria cardamomum (L.) Maton essential oil: an interesting source of bioactive specialized metabolites as inhibitors of acetylcholinesterase and butyrylcholinesterase. Plants. 2023;12(19).

[16] Sahoo S, Jyotirmayee B, Nayak S, Samal HB, Mahalik G. Review on phytopharmacological activity of Curcuma amada Roxb. (mango ginger). Def Life Sci J. 2023;8(4):351-62.

[17] Qian S, Cheng X, Song W, Zheng Y, Tang R, Fan J, et al. An integrated hydrothermal-enzymatic biorefinery approach for efficient ferulic acid production from Euryale ferox seed shell via lignin removal. Process Biochem. 2026;162:74-82.

[18] Huang Y, Liu Y, Tan H, Cheng Y, Tao K, Gu D, et al. Assessing essential oil composition in Cinnamomum cassia leaves from different regions of China using GC-MS and FTIR spectroscopy. Czech J Food Sci. 2024;42(3):141-52.

[19] Ebrahimi A, Asadi AA, Monfared SR, Sahebi M, Rezaee S, Khaledian Y. Evaluation of phenotypic diversity of the endangered orchid (Orchis mascula): emphasizing on breeding, conservation and development. South African J Bot. 2020;132:304-15.

[20] Ala-Jaakkola R, Laitila A, Ouwehand AC, Lehtoranta L. Role of D-mannose in urinary tract infections – a narrative review. Nutr J. 2022;21(1).

[21] Malakotikhah F, Shahanipour K, Monajemi R, Ahadi AM, Rastegari AA. Study the impact of galangin and Alpinia galanga L. on the activation of apoptosis in breast cancer. Cytotechnology. 2025;77(3).

[22] Pathak R, Sharma H. A review on medicinal uses of Cinnamomum verum (cinnamon). J Drug Deliv Ther. 2021;11(6-S):161-6.

[23] Kim JE, Park KH, Park J, Kim BS, Kim GS, Hwang DG. Immunomodulatory potential of 6-gingerol and 6-shogaol in Lactobacillus plantarum-fermented Zingiber officinale extract on murine macrophages. Int J Mol Sci. 2025;26(5).

[24] Champati BB, Padhiari BM, Ray A, Jena S, Sahoo A, Mohanty S, et al. Implementation of multilayer perceptron (MLP) and radial basis function (RBF) neural networks for predicting Shatavarin IV content in Asparagus racemosus accessions. Ind Crops Prod. 2023;191.

[25] Chacón-Guzmán J, Carvajal-Oses M, Pauletto S, Herrera-Ulloa Á. Concentration and maximum exposure time of Lutjanus guttatus juveniles to Syzygium aromaticum eugenol. Rev Ciencias Mar y Costeras. 2019;11(1):9-25.

[26] Dwivedi V, Maurya H. A comprehensive overview of Celastrus paniculatus seed oil intended for the management of human ailments. Indian J Pharm Biol Res. 2018;6(02):37-42.

[27] Rao RN, Raju SS, Babu KS, Vadaparthi PRR. HPLC determination of costunolide as a marker of Saussurea lappa and its herbal formulations. Int J Res Pharm Chem. 2013;3(1):99-107.

[28] Gnanaraj M, Sivamaruthi BS, Mohamed SS, Sisubalan N, Basha MHG, Chaiyasut C. Optimization of conditions to achieve a high content of alizarin and purpurin in the adventitious roots of Rubia cordifolia L. J Appl Biol Biotechnol. 2025;13(1):150-8.

[29] Medic A, Zamljen T, Slatnar A, Hudina M, Veberic R. Is juglone the only naphthoquinone in Juglans regia L. with allelopathic effects? Agric. 2021;11(8).

[30] Shalayel MHF, Al-Mazaideh GM, Alanezi AA, Almuqati AF, Alotaibi M. The potential anti-cancerous activity of

Prunus amygdalus var. amara extract. Processes. 2023;11(4).
[31] Nitbani FO, Jumina, Siswanta D, Solikhah EN. Isolation and antibacterial activity test of lauric acid from crude coconut oil (Cocos nucifera L.). Procedia Chem. 2016;18:132-40.
[32] Khedkar SM, Barvkar VT, Sardesai MM, Kotkar HM. Profiling of saponins in four different species of Chlorophytum by liquid chromatography quadrupole time of flight mass spectrometry. Nat Prod Res. 2025;39(15):4493-6.
[33] Znad OS, Zghair ZR. Antimicrobial activity of aloe-emodin from Aloe vera against Staphylococcus aureus. J Pak Med Assoc. 2023;73(9):S124-8.
[34] Karasawa K, Uzuhashi Y, Hirota M, Otani H. A matured fruit extract of date palm tree (Phoenix dactylifera L.) stimulates the cellular immune system in mice. J Agric Food Chem. 2011;59(20):11287-93.
[35] Tamboli AS, Tayade SD. In-depth investigation of berberine and tropane through computational screening as possible DPP-IV inhibitors for the treatment of T2DM. J Pharm Sci Comput Chem. 2025;1(1):1-11.
[36] Hani U, Al-Qahtani EH, Albeeshi FF, Alshahrani SS. Exploring the landscape of drug-target interactions: molecular mechanisms, analytical approaches, and case studies. J Pharm Sci Comput Chem. 2025;1(1):12-25.
[37] Sadikova U. Computational study of alkaloids transferase as antidiabetic agents targeting. J Phytopharm Adv Chem. 2026;1(1):18-29.
[38] Siddiqui FS. Computational assessment of secondary metabolites as potential inhibitors of methylenetetrahydrofolate dehydrogenase-2 (MTHFD2). J Phytopharm Adv Chem. 2026;1(1):3-17.
[39] Orlu HA, Ajoko IT, Felagha I, Nwajei EC, Ebong CU. In silico evaluation of ADMET properties and drug-likeness of bioactive compounds from Citrullus colocynthis seed oil targeting human superoxide dismutase. Med Med Chem. 2025;2:177-93.
[40] Jadhav SS, Dighe PR, Kumbhare MR. Synthesis, in vitro evaluation, and molecular docking studies of novel pyrazoline derivatives as promising bioactive molecules. J Pharm Sci Comput Chem. 2025;1(3).
[41] Khan SL, Bakshi V. LC-HRMS and in silico analysis of Ailanthus excelsa metabolites targeting EGFR triple mutation (L858R/T790M/C797S). Adv J Chem Sect A. 2026;9(2):292-311.
[42] Roy D. Drug repurposing of some US FDA-approved drugs using binding strength studies for the treatment of methicillin-resistant Staphylococcus aureus infection. J Phytopharm Adv Chem. 2026;1(1):30-44.
[43] Siddiqui FA, Bakshi V. GC–MS-based analytical profiling of Lantana camara phytoconstituents and computational analysis for multi-target antidiabetic activity. J Chem Lett. 2026;7(1):1-24.
[44] Gandla K, Islam F, Zehravi M, Karunakaran A, Sharma I, Haque MA, et al. Natural polymers as potential P-glycoprotein inhibitors: pre-ADMET profile and computational analysis as a proof of concept to fight multidrug resistance in cancer. Heliyon. 2023;9(9).
[45] Shastri MA, Gadhave R, Talath S, Wali AF, Hani U, Puri S, et al. In silico screening, synthesis, and in vitro enzyme assay of some 1,2,3-oxadiazole-linked tetrahydropyrimidine-5-carboxylate derivatives as DPP-IV inhibitors for treatment of T2DM. Chem Methodol. 2024;8(11):800-19.
[46] Sadikova U. Computational study of alkaloids targeting O-GlcNAc transferase as antidiabetic agents. J Phytopharm Adv Chem. 2026;1(1):18-29.
[47] Khan SL, Bakshi V. Physicochemical characterization, GC–MS profiling, and computational evaluation of Ailanthus excelsa hydroalcoholic extract against mutant EGFR. Chem Rev Lett. 2026;9(2):358-76.